PERGAMON

International Journal of Heat and Mass Transfer 44 (2001) 3241–3251

International Journal of HEAT and MASS TRANSFER

www.elsevier.com/locate/ijhmt

Transient force and free convection along a vertical wavy surface in micropolar fluids

Chi-Chang Wang, Cha'o-Kuang Chen *

Department of Mechanical Engineering, National Cheng Kung University, Tainan, Taiwan 70701, People's Republic of China

Received 22 May 2000; received in revised form 17 October 2000

Abstract

This work studies the transient behavior of the laminar mixed convection in micropolar fluid flow over a vertical wavy surface. Effects of micropolar parameters and wavy geometry on the transient skin friction coefficient and Nusselt number are examined. Results show that the transient skin-friction coefficient and heat transfer rate show a mixture of two harmonics. Forced convection dominates the first harmonic at smaller time or near the leading edge, while free convection dominates the second harmonic as the time increases and fluid moves downstream. As the vortex viscosity increases the Nusselt number decreases, thus micropolar fluids have smaller heat transfer rates.

Keywords: Micropolar fluid; Mixed convection; Wavy surface

1. Introduction

The theory of micropolar fluid can be used to explain the flow behavior of non-Newtonian fluids, such as colloidal fluids, polymeric fluids, animal blood and real fluids with suspensions. This theory, first formulated by Eringen [1], could deal with viscous fluids where the microconstituents are rigid and spherical or randomly oriented. It has received much attention in recent years. An excellent review about micropolar fluids was provided by Ariman et al. [2,3].

It is necessary to study the heat transfer from irregular surfaces because irregular surfaces are often present in many applications. Surfaces are sometimes intentionally roughened to enhance heat transfer. Mixed convection from wavy surfaces can be used for transferring heat in several heat transfer devices, such as flat-plate solar collectors and flat-plate condensers in refrigerators. The presence of roughness elements disturbs the flow pass surfaces and alters the heat transfer rate. Previous studies about the mixed convection of micropolar fluid flows have focused mainly on a flat plate [4]. Few studies have considered the effects of complex geometries on heat convection in micropolar fluids, including the flows along a convex surface [5] and Stretching Sheet [6]. Yao [7–9] first studied the natural convection flow of Newtonian fluid along a vertical wavy surface using an extended Prandtl's transposition theorem and a finite-difference scheme. Pop et al. [10,11] investigated the free convection along a vertical wavy surface in a porous medium and natural convection of a Darcian fluid about a wavy cone. And recently, Pop et al. [12,13] studied the transient conjugate free convection from a vertical plate subjected to a change in surface heat flux in porous media by an explicit finite-difference scheme. Chiu et al. [14,15] studied the transient and steady-state natural convection along a vertical wavy surface in micropolar fluids. They found that the frequency of the local heat transfer rate and the skin friction on the wall are twice that of the wavy surface irrespective of whether the fluid is a Newtonian fluid or micropolar fluid. About the mixed-convection along a vertical wavy surface, Yao [16] showed that the forced-convection component of the heat transfer contains two harmonics. The amplitude of the first harmonic is proportional to the amplitude of the wavy surface, and the natural-convection component is a second harmonic, with a frequency twice that of the wavy surface.

* Corresponding author. Tel.: +1-886-6-275-7575; fax: +1-886-6-234-2081.

E-mail address: ckchen@mail.ncku.edu.tw (C.-K. Chen).

0017-9310/01/$ - see front matter
PII: S0017-9310(00)00329-X

Nomenclature

a	dimensionless amplitude of the wavy surface
B	dimensionless material parameter (Eq. (2))
C_f	skin friction coefficient
C_p	specific heat of the fluid at constant pressure
g	acceleration due to gravity
Gr	Grashof number (Eq. (2))
h	heat transfer coefficient
j	micro-inertia density
K_f	thermal conductivity
L	wavy length
N	dimensionless microrotation
$Nu_{\bar{x}}, Nu_m$	local Nusselt number, and mean Nusselt number, respectively
p	pressure
Pr	Prandtl number
R	dimensionless micropolar parameter (Eq. (2))
Re	generalized Reynolds number
S	surface geometry function
T	temperature
t	time
u, v	x and y velocity components, respectively
U_∞	x component of the velocity of the inviscid flow, evaluated at the surface
x, y	axial and transverse (Cartesian) coordinates, respectively

Greek symbols

α	wavy amplitude–wavelength ratio
λ	material parameter ($\gamma/j\mu$)
σ	distance measured along the surface from the leading edge
θ	dimensionless temperature
μ	dynamic viscosity
v_3	microrotation component
β	coefficient of thermal expansion
γ	spin gradient viscosity
ρ	density of fluid
τ	dimensionless time

Superscripts

$-$	dimensional quantity
$\sim$, $\wedge$	non-dimensional quantity
$'$	derivative with respect to x

Subscripts

m	mean value
x	local value
w	surface conditions
∞	conditions far away from the surface

The above literature survey shows that the transient mixed convection along a vertical wavy surface, especially in micropolar fluids, has not been studied so far. In this paper we analyze the transient mixed convection in micropolar fluid flows over a vertical wavy surface using Prandtl's transposition theorem and the spline alternating-direction implicit method. The gradient boundary conditions can be represented more accurately, and irregular boundaries are easier to deal with. This is because the spline alternating-direction implicit method can directly evaluate the spatial derivative terms without any finite-difference discretization. The analysis needs to know the inviscid flow along the wavy surface and the inviscid solution obtained in this paper is valid only for small values of the amplitude–wavelength ratio. We examine the effects of micropolar parameters and wavy geometry on the profiles of velocity, temperature, microrotation, skin-friction coefficient and Nusselt number. Results obtained are also compared with the corresponding flow in Newtonian fluids.

2. Mathematical formulation

Consider a wavy surface, having a cusped leading edge as shown in Fig. 1. The axis of symmetry is aligned with the oncoming uniform stream. The wavy surface is described by $\bar{S}(\bar{x}) = \bar{a}\sin^2(\pi\bar{x}/L)$, where $\bar{a}$ is the amplitude of the wavy surface. We assume that the temperature of the wavy surface is held at a constant value T_w, which is higher than the ambient fluid temperature T_∞. Moreover, the micropolar fluid flow is consider to be transient, laminar and two-dimensional. The governing equations can be written under the Boussinesq approximation as

$$\frac{\partial\bar{u}}{\partial\bar{x}} + \frac{\partial\bar{v}}{\partial\bar{y}} = 0, \tag{1a}$$

$$\rho\left(\frac{\partial\bar{u}}{\partial t} + \bar{u}\frac{\partial\bar{u}}{\partial\bar{x}} + \bar{v}\frac{\partial\bar{u}}{\partial\bar{y}}\right) = -\frac{\partial\bar{p}}{\partial\bar{x}} + (\mu+\kappa)\left(\frac{\partial^2\bar{u}}{\partial\bar{x}^2} + \frac{\partial^2\bar{u}}{\partial\bar{y}^2}\right) + \rho g\beta(T - T_\infty) + \kappa\frac{\partial v_3}{\partial\bar{y}}, \tag{1b}$$

$$\rho\left(\frac{\partial\bar{v}}{\partial t} + \bar{u}\frac{\partial\bar{v}}{\partial\bar{x}} + \bar{v}\frac{\partial\bar{v}}{\partial\bar{y}}\right) = -\frac{\partial\bar{p}}{\partial\bar{y}} + (\mu+\kappa)\left(\frac{\partial^2\bar{v}}{\partial\bar{x}^2} + \frac{\partial^2\bar{v}}{\partial\bar{y}^2}\right) + \kappa\left(-\frac{\partial v_3}{\partial\bar{x}}\right), \tag{1c}$$

$$\rho j\left(\frac{\partial v_3}{\partial t} + \bar{u}\frac{\partial v_3}{\partial\bar{x}} + \bar{v}\frac{\partial v_3}{\partial\bar{y}}\right) = \kappa\left(\frac{\partial\bar{v}}{\partial\bar{x}} - \frac{\partial\bar{u}}{\partial\bar{y}} - 2v_3\right) + \gamma\left(\frac{\partial^2 v_3}{\partial\bar{x}^2} + \frac{\partial^2 v_3}{\partial\bar{y}^2}\right), \tag{1d}$$

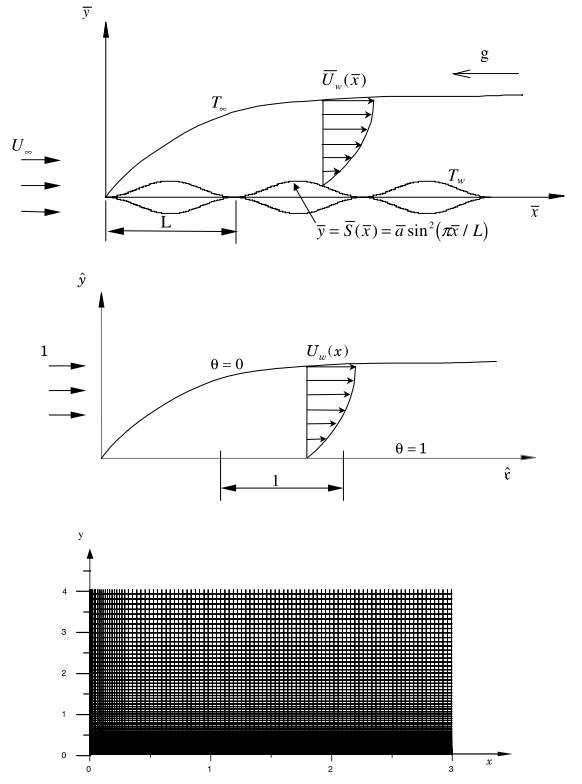

Fig. 1. Physical model, coordinates and grid system.

$$\rho C_p\left(\frac{\partial T}{\partial t}+\bar{u}\frac{\partial T}{\partial \bar{x}}+\bar{v}\frac{\partial T}{\partial \bar{y}}\right)=K_f\left(\frac{\partial^2 T}{\partial \bar{x}^2}+\frac{\partial^2 T}{\partial \bar{y}^2}\right). \tag{1e}$$

The initial condition is

$$t=0: T(\bar{x},\bar{y},0)=0,\quad \bar{u}(\bar{x},\bar{y},0)=0,\quad v_3(\bar{x},\bar{y},0)=0. \tag{1f}$$

Moreover, the associate boundary conditions are

$$\text{(1) At } \bar{y}=\bar{S}(\bar{x}),\quad t>0: T=T_w,\ \bar{u}=\bar{v}=0,\ v_3=0, \tag{1g}$$

$$\text{(2) At } \bar{y}\to\infty,\quad t>0: T=T_\infty,\ \bar{u}=\bar{U}_w(\bar{x}),\ v_3=0,\ \bar{p}=\bar{p}_\infty(\bar{x}). \tag{1h}$$

Note that $\bar{u}$ and $\bar{v}$ are the components of the velocity along the $\bar{x}$, $\bar{y}$ directions. T, $\bar{p}$, and g are the temperature, pressure and gravitational constant. ρ, μ and β are the density, viscosity and thermal expansion coefficient of fluid. j, κ and γ are the micro-inertia density, vortex viscosity and spin-gradient viscosity. Further, K_f and C_p are the thermal conductivity and specific heat of the fluid at constant pressure. v_3 is the component of microrotation whose direction of rotation is in the $(x$–$y)$ plane. $\bar{U}_w(\bar{x})$ is the $\bar{x}$ component of the inviscid velocity at the surface $\bar{y}=\bar{S}(\bar{x})$.

Note that in Eq. (1g), the boundary condition for the microrotation at the fluid–solid interface is $v_3=0$, the condition of zero spin, as used by Takhar [6].

The dimensionless variables are defined as

$$\tilde{x}=\frac{\bar{x}}{L},\quad \tilde{y}=\frac{\bar{y}}{L},\quad \tilde{\tau}=\frac{\bar{t}U_\infty}{L},\quad \alpha=\frac{\bar{a}}{L},$$
$$S(\tilde{x})=\frac{\bar{S}(\bar{x})}{L},\quad \tilde{u}=\frac{\bar{u}}{U_\infty},\quad \tilde{v}=\frac{\bar{v}}{U_\infty},\quad \tilde{N}=\frac{v_3 L}{U_\infty},$$
$$\theta=\frac{T-T_\infty}{T_w-T_\infty},\quad U_w=\frac{\bar{U}_w}{U_\infty},\quad \tilde{p}=\frac{\bar{p}}{\rho U_\infty^2},$$
$$B=\frac{L\mu}{j\rho U_\infty},\quad \lambda=\frac{\gamma}{\mu j},\quad R=\frac{\kappa}{\mu},\quad Re=\frac{\rho U_\infty L}{\mu},$$
$$Pr=\frac{\mu C_p}{K_f},\quad Gr=\frac{g\beta(T_w-T_\infty)\rho^2 L^3}{\mu^2}. \tag{2}$$

Substitution of Eq. (2) into Eqs. (1a)–(1e) yields

$$\frac{\partial\tilde{u}}{\partial\tilde{x}}+\frac{\partial\tilde{v}}{\partial\tilde{y}}=0, \tag{3a}$$

$$\frac{\partial\tilde{u}}{\partial\tilde{\tau}}+\tilde{u}\frac{\partial\tilde{u}}{\partial\tilde{x}}+\tilde{v}\frac{\partial\tilde{u}}{\partial\tilde{y}}=-\frac{\partial\tilde{p}}{\partial\tilde{x}}+\frac{1+R}{Re}\left(\frac{\partial^2\tilde{u}}{\partial\tilde{x}^2}+\frac{\partial^2\tilde{u}}{\partial\tilde{y}^2}\right)+\frac{Gr}{Re^2}\theta+\frac{R}{Re}\frac{\partial\tilde{N}}{\partial\tilde{y}}, \tag{3b}$$

$$\frac{\partial\tilde{v}}{\partial\tilde{\tau}}+\tilde{u}\frac{\partial\tilde{v}}{\partial\tilde{x}}+\tilde{v}\frac{\partial\tilde{v}}{\partial\tilde{y}}=-\frac{\partial\tilde{p}}{\partial\tilde{y}}+\frac{1+R}{Re}\left(\frac{\partial^2\tilde{v}}{\partial\tilde{x}^2}+\frac{\partial^2\tilde{v}}{\partial\tilde{y}^2}\right)+\frac{R}{Re}\left(-\frac{\partial\tilde{N}}{\partial\tilde{x}}\right) \tag{3c}$$

$$\frac{\partial\tilde{N}}{\partial\tilde{\tau}}+\tilde{u}\frac{\partial\tilde{N}}{\partial\tilde{x}}+\tilde{v}\frac{\partial\tilde{N}}{\partial\tilde{y}}=RB\left(\frac{\partial\tilde{v}}{\partial\tilde{x}}-\frac{\partial\tilde{u}}{\partial\tilde{y}}-2\tilde{N}\right)+\frac{\lambda}{Re}\left(\frac{\partial^2\tilde{N}}{\partial\tilde{x}^2}+\frac{\partial^2\tilde{N}}{\partial\tilde{y}^2}\right), \tag{3d}$$

$$\frac{\partial\theta}{\partial\tilde{\tau}}+\tilde{u}\frac{\partial\theta}{\partial\tilde{x}}+\tilde{v}\frac{\partial\theta}{\partial\tilde{y}}=\frac{1}{RePr}\left(\frac{\partial^2\theta}{\partial\tilde{x}^2}+\frac{\partial^2\theta}{\partial\tilde{y}^2}\right). \tag{3e}$$

Using Prandtl's transposition theorem, we can transform the irregular wavy surface into a flat surface [8]. The transformed equations are

$$\frac{\partial\hat{u}}{\partial\hat{x}}+\frac{\partial\hat{v}}{\partial\hat{y}}=0, \tag{4a}$$

$$\frac{\partial\hat{u}}{\partial\hat{\tau}}+\hat{u}\frac{\partial\hat{u}}{\partial\hat{x}}+\hat{v}\frac{\partial\hat{u}}{\partial\hat{y}}=-\frac{\partial\hat{p}}{\partial\hat{x}}+Re^{1/2}S'\frac{\partial\hat{p}}{\partial\hat{y}}+(1+R)\left(1+S'^2\right)\frac{\partial^2\hat{u}}{\partial\hat{y}^2}+\frac{Gr}{Re^2}\theta+R\frac{\partial\hat{N}}{\partial\hat{y}}, \tag{4b}$$

$$\hat{u}^2 S'' + S' \frac{Gr}{Re^2}\theta = S' \frac{\partial \hat{p}}{\partial \hat{x}} - Re^{1/2}(1+S'^2)\frac{\partial \hat{p}}{\partial \hat{y}}, \tag{4c}$$

$$\frac{\partial \hat{N}}{\partial \hat{\tau}} + \hat{u}\frac{\partial \hat{N}}{\partial \hat{x}} + \hat{v}\frac{\partial \hat{N}}{\partial \hat{y}} = RB\left[-(1+S'^2)\frac{\partial \hat{u}}{\partial \hat{y}} - 2\hat{N}\right] + \lambda(1+S'^2)\frac{\partial^2 \hat{N}}{\partial \hat{y}^2}, \tag{4d}$$

$$\frac{\partial \theta}{\partial \hat{\tau}} + \hat{u}\frac{\partial \theta}{\partial \hat{x}} + \hat{v}\frac{\partial \theta}{\partial \hat{y}} = \frac{1}{Pr}(1+S'^2)\frac{\partial^2 \theta}{\partial \hat{y}^2}, \tag{4e}$$

where

$$\hat{x} = \tilde{x}, \quad \hat{y} = (\tilde{y} - S(\tilde{x}))Re^{1/2}, \quad \hat{\tau} = \tilde{\tau}, \hat{u} = \tilde{u}, \\ \hat{v} = (\tilde{v} - S'\tilde{u})Re^{1/2}, \quad \hat{N} = \tilde{N}Re^{-1/2}, \quad \hat{p} = \tilde{p} - \tilde{p}_\infty. \tag{5}$$

Eq. (4c) indicates that $\partial\hat{p}/\partial\hat{y}$ is $O(Re^{-1/2})$. This implies that the $\partial\hat{p}/\partial\hat{x}$ can be determined from the inviscid flow in the outside of the boundary layer. It can be expressed as:

$$\frac{\partial \hat{p}}{\partial \hat{x}} = -[(1+S'^2)U_w U'_w + S'S''U_w^2]. \tag{6}$$

Elimination of $\partial\hat{p}/\partial\hat{y}$ between Eqs. (4b) and (4c) yields

$$\frac{\partial \hat{u}}{\partial \hat{\tau}} + \hat{u}\frac{\partial \hat{u}}{\partial \hat{x}} + \hat{v}\frac{\partial \hat{u}}{\partial \hat{y}} = \frac{1}{1+S'^2}\left(\frac{Gr}{Re^2}\theta - \frac{\partial \hat{p}}{\partial \hat{x}} - S'S''\hat{u}^2\right) + (1+R)(1+S'^2)\frac{\partial^2 \hat{u}}{\partial \hat{y}^2} + R\frac{\partial N}{\partial \hat{y}}. \tag{7}$$

Here, we defined the following variables

$$x = \hat{x}, \quad y = \hat{y}\left(\frac{2\hat{x}}{U_w}\right)^{-1/2}, \quad \tau = \hat{\tau}\left(\frac{2\hat{x}}{U_w}\right)^{-1}, \\ u = \frac{\hat{u}}{U_w}, \quad v = \hat{v}\left(\frac{2\hat{x}}{U_w}\right)^{1/2}, \quad N = \hat{N}\left(\frac{2\hat{x}}{U_w}\right)^{1/2}. \tag{8}$$

The boundary layer Eqs. (4a), (4d), (4e) and (7) in (x,y) coordinates are

$$2x\frac{\partial u}{\partial x} - y\left(1 - x\frac{U'_w}{U_w}\right)\frac{\partial u}{\partial y} + \frac{\partial v}{\partial y} + 2x\frac{U'_w}{U_w}u = 0, \tag{9a}$$

$$\frac{\partial u}{\partial \tau} + 2xu\frac{\partial u}{\partial x} + \left[v - yu\left(1 - x\frac{U'_w}{U_w}\right)\right]\frac{\partial u}{\partial y} + 2x(u^2-1)\left(\frac{S'S''}{1+S'^2} + \frac{U'_w}{U_w}\right) = \frac{2x}{U_w^2(1+S'^2)}\frac{Gr}{Re^2}\theta + (1+R)(1+S'^2)\frac{\partial^2 u}{\partial y^2} + \frac{R}{U_w}\frac{\partial N}{\partial y}, \tag{9b}$$

$$\frac{\partial N}{\partial \tau} + 2xu\frac{\partial N}{\partial x} + \left[v - yu\left(1 - x\frac{U'_w}{U_w}\right)\right]\frac{\partial N}{\partial y} - uN\left(1 - x\frac{U'_w}{U_w}\right) = xRB\left[-2(1+S'^2)\frac{\partial u}{\partial y} - 4\frac{N}{U_w}\right] + \lambda(1+S'^2)\frac{\partial^2 N}{\partial y^2}, \tag{9c}$$

$$\frac{\partial \theta}{\partial \tau} + 2xu\frac{\partial \theta}{\partial x} + \left[v - yu\left(1 - x\frac{U'_w}{U_w}\right)\right]\frac{\partial \theta}{\partial y} = \frac{1+S'^2}{Pr}\frac{\partial^2 \theta}{\partial y^2}. \tag{9d}$$

The corresponding initial and boundary conditions are:

$$\tau = 0 : \theta = 0, \ \ u = 0, \ \ N = 0, \tag{9e}$$

$$y = 0, \ \ \tau > 0 : \theta = 1, \ \ u = v = 0, \ \ N = 0, \tag{9f}$$

$$y \to \infty, \ \ \tau > 0 : \theta = 0, \ \ u = 1, \ \ N = 0. \tag{9g}$$

The potential-flow solution for x-component of the velocity on the surface $y = S(x)$ can expressed as [16]

$$U_w(x) = 1 + \frac{1}{\pi}\int_0^\infty \frac{S'(t)}{x-t}\,dt + O(\alpha^2). \tag{10a}$$

Removing the singular point of the integral by the residue theorem yields

$$U_w(x) = 1 + a\left[-\pi\cos(2\pi x) + \int_0^\infty \frac{\sin(2\pi t)}{x+t}\,dt\right] + O(\alpha^2). \tag{10b}$$

The local Nusselt number is defined as:

$$Nu_{\bar{x}} = \frac{h_{\bar{x}}\bar{x}}{K_f} = \frac{(-\partial T/\partial n)\bar{x}}{T_w - T_\infty}, \tag{11a}$$

where

$$\frac{\partial T}{\partial n} = \sqrt{\left(\frac{\partial T}{\partial \bar{x}}\right)^2 + \left(\frac{\partial T}{\partial \bar{y}}\right)^2}. \tag{11b}$$

Here $\partial/\partial n$ represents the differentiation with respect to the coordinate normal to the surface. The axial distribution of $(4/Gr_{\bar{x}})^{1/4}Nu_{\bar{x}}$ can be obtained from

$$\left(\frac{4}{Gr_{\bar{x}}}\right)^{1/4}Nu_{\bar{x}} = -\left(\frac{Gr}{Re^2}\right)^{-1/4}\left[(1+S'^2)U_w\right]^{1/2}\left.\frac{\partial \theta}{\partial y}\right|_{y=0}. \tag{11c}$$

The mean Nusselt number is defined as:

$$Nu_m = \frac{h_m \bar{x}}{K_f}. \tag{12a}$$

We can calculate the value of $(4/Gr_{\bar{x}})^{1/4}Nu_{\bar{x}}$ from

$$\left(\frac{4}{Gr_{\bar{x}}}x\right)^{1/4}Nu_m = \left(\frac{Gr}{Re^2}x\right)^{-1/4}\frac{-(2x)^{1/2}}{\sigma} \times \int_0^\infty \left(\frac{U_w}{2x}\right)^{1/2}(1+S'^2)\left.\frac{\partial \theta}{\partial y}\right|_{y=0} dx, \tag{12b}$$

where

$$h_m = \frac{q_m}{T_w - T_\infty}, \tag{12c}$$

$$q_m = \frac{1}{\sigma}\int_0^\sigma -K_f \frac{\partial T}{\partial n}\,d\sigma, \tag{12d}$$

$$\sigma = \int_0^x (1 + S'2)^{1/2}\,dx. \tag{12e}$$

The shear force at the surface is

$$\tau_w = \left[\mu\left(\frac{\partial \bar{u}}{\partial \bar{y}} + \frac{\partial \bar{v}}{\partial \bar{x}}\right) + \kappa\left(\frac{\partial \bar{u}}{\partial \bar{y}} + v_3\right)\right]_{\bar{y}=\bar{S}(\bar{x})}. \tag{13a}$$

Finally the skin-friction coefficient C_f can be defined as

$$C_f = \frac{2\tau_w}{\rho U_w^2}. \tag{13b}$$

Substitution of Eq. (13a) into Eq. (13b) and ignoring the small order terms yields

$$\left(\frac{Gr}{Re^2}\right)^{-1}\left(\frac{Gr}{4x}\right)^{1/4} C_f = \frac{1}{2}\left(\frac{Gr}{Re^2}x\right)^{-3/4}(2+R) \times U_w^{3/2}(1 - S'^2)\frac{\partial u}{\partial y}. \tag{13c}$$

3. Numerical method

The dimensionless governing differential Eqs. (9a)–(9c) combined with the relevant boundary conditions Eqs. (9e)–(9g) are solved numerically by the spline alternating-direction implicit method [18,19], an improved version of the cubic spline collocation method [17]. Numerical experiments were carried out to ensure the independence of the results on the grid spacing and time step size. Table 1 presents the results of the local Nusselt number and local skin-friction coefficient. The difference between results for spatial grids of 250×50 and 500×125 is less than 0.07% in the local Nusselt number and the local skin-friction coefficient for $Pr = 1.0, \alpha = 0.1, Gr/Re^2 = 20\pi$, $x \in [0,4]$ and $y \in [0,8]$. The difference between results for $\Delta\tau = 0.01$ and $\Delta\tau = 0.001$ is less than 0.2% in the transient local Nusselt number and the transient skin-friction coefficient, when a non-uniform 250×50 grid is used. Therefore, we employ a time interval $\Delta\tau = 0.01$ and a non-uniform grid (250×50) to calculate the results. Smaller spacing mesh points are used in the neighborhood of the fluid–solid boundary in y direction, as well as near the leading edge in x direction, as shown in Fig. 1.

Using the spline alternating-direction implicit method, we can express Eqs. (9a)–(9g) as

$$\varphi_{i,j}^{n+1} = F_{i,j} + G_{i,j}m_{i,j}^{n+1} + S_{i,j}M_{i,j}^{n+1}. \tag{14}$$

Here i and j refer to the computational nodes, and n is the time step. Moreover, φ represents u, v, N and θ. m and M are the first and second derivatives of φ with respect to x and y, respectively. $F_{i,j}$, $G_{i,j}$ and $S_{i,j}$ are the known coefficients evaluated at the previous time step, as show in Table 2. Using cubic spline collocation

Table 1
Comparison of $4/Gr_{\bar{x}})^{1/4}Nu_{\bar{x}}$ and $(Gr/Re^2)^{-1}(Gr/4x)^{1/4}C_f$ for $Pr = 1.0, \alpha = 0.1, Gr/Re^2 = 20\pi, R = 0, x \in [0,4], y \in [0,8]$: (a) for different grid sizes; (b) for different time steps

	$\left(\frac{4}{Gr_{\bar{x}}}\right)^{1/4} Nu_{\bar{x}}$		$\left(\frac{Gr}{Re^2}\right)^{-1}\left(\frac{Gr}{4x}\right)^{1/4} C_f$	
	$x = 0.3$	$x = 4$	$x = 0.3$	$x = 4$
(a) Steady-state solutions: $\Delta\tau = 0.01$				
250×25	0.583117	0.561775	1.121591	1.288961
250×50	0.583923	0.563652	1.118965	1.284000
250×125	0.584239	0.564578	1.118137	1.282617
125×50	0.585460	0.563947	1.117896	1.284542
250×50	0.583923	0.563652	1.118965	1.284000
500×125	0.583643	0.564079	1.119068	1.283798
250×50[a]	0.584834	0.563722	1.120845	1.283808
250×50[b]	0.599158	0.604465	1.119762	1.273850
(b) Unsteady-state solution: grid sizes $= 250 \times 50, \tau = 0.4$				
$\Delta\tau = 0.001$	0.583922	0.752781	1.118966	0.898207
$\Delta\tau = 0.010$	0.583924	0.752782	1.118966	0.898219
$\Delta\tau = 0.050$	0.583925	0.752723	1.118968	0.897970
$\Delta\tau = 0.100$	0.583927	0.752636	1.118974	0.895481

[a] Uniform grid (x direction).
[b] Uniform grid (y direction).

Table 2
The value of $F_{i,j}$, $G_{i,j}$, and $S_{i,j}$

u	$F_{i,j}$	$u_{i,j}^{n} + \Delta\tau\Big[-2xu_{i,j}^{n+1}(\partial u/\partial x)^{n+1} - 2x((u_{i,j}^{n+1})^2 - 1)\left(\frac{S'S''}{1+S'^2} + \frac{U_w'}{U_w}\right) + 2xU_w^2(1+S')\frac{Gr}{Re}\theta + \frac{R}{U_w}I_N^{n+1}\Big]$
	$G_{i,j}$	$-\Delta\tau\left[v_{i,j}^{n+1} - y_j u_{i,j}^{n+1}\left(1 - x\frac{U_w'}{U_w}\right)\right]$
	$S_{i,j}$	$\Delta\tau(1+R)(1+S'^2)$
N	$F_{i,j}$	$N_{i,j}^{n} + \Delta\tau\Big[-2xu_{i,j}^{n+1}\left(\frac{\partial N}{\partial x}\right)^{n+1} + \left(1 - x\frac{U_w'}{U_w}\right)u_{i,j}^{n+1} + RBx\left(-2(1+S'^2)I_u^{n+1} - 4 + \frac{N^{n+1}}{U_w}\right)\Big]$
	$G_{i,j}$	$-\Delta\tau\left[v_{i,j}^{n+1} - y_j u_{i,j}^{n+1}\left(1 - x\frac{U_w'}{U_w}\right)\right]$
	$S_{i,j}$	$\Delta\tau\lambda(1+S'^2)$
θ	$F_{i,j}$	$\theta_{i,j}^{n} + \Delta\tau\left[-2xu_{i,j}^{n+1}\left(\frac{\partial\theta}{\partial x}\right)^{n+1}\right]$
	$G_{i,j}$	$-\Delta\tau\left[v_{i,j}^{n+1} - y_j u_{i,j}^{n+1}\left(1 - x\frac{U_w'}{U_w}\right)\right]$
	$S_{i,j}$	$\frac{\Delta\tau}{P_r}(1+S'^2)$

relations [17], we can express Eq. (14) in tridiagonal form as

$$A_{i,j}\phi_{i,j}^{n+1} + B_{i,j}\phi_{i,j}^{n+1} + C_{i,j}\phi_{i,j}^{n+1} = D_{i,j}, \tag{15}$$

where ϕ represents u, v, N and θ, or its first two derivatives. Eq. (15) can be easily solved by the Thomas algorithm.

The numerical procedure is as follows.

1. Set the suitable boundary and initial conditions.
2. Solve the transient solution from the leading edge. At every axial position, the inner iterations for convergent solutions are performed in every time step until the convergence criteria are satisfied, that

$$\left|\frac{\phi_{i,j}^{z+1} - \phi_{i,j}^{z}}{\phi_{i,j}^{z+1}}\right| \leqslant 1 \times 10^{-5},$$

where ϕ refers to θ, u, v or N, and z denotes the number of iterations.

3. Go back to step 2 to calculate the results for the next time step. The solutions obtained are treated as steady-state solutions when the criteria are satisfied, i.e.,

$$\left|\frac{\phi_{i,j}^{n+1} - \phi_{i,j}^{n}}{\phi_{\max}^{n+1}}\right| < 1 \times 10^{-6},$$

where n denotes the number of time steps.

4. Results and discussion

Numerical results are obtained for the surface described by $S(\bar{x}) = \bar{a}\sin^2(\pi\bar{x}/L)$ or dimensionless $S(x) = \alpha\sin^2(\pi x)$ for amplitude–wavelength ratios of 0.1 and 0.2. The effects of governing physical parameters, such as amplitude–wavelength ratios α, and material parameters R are examined. The typical chosen values are $B = 1, \lambda = 5, Pr = 1$ and $Gr/Re^2 = 20\pi$.

Results for Eqs. (6) and (10b) are plotted in Fig. 2. Fig. 2 shows that the flow accelerates along the portion of the surface from trough to crest where the slop S' is positive, and it decelerates along the portion of the surface from crest to trough where the slope S' is negative. The x-component velocity of the inviscid flow U_w varies periodically along the surface with a cycle equal to that of the wavy surface. Moreover, this velocity increases with the amplitude–wavelength ratio. On the other hand, Fig. 3 shows that the pressure gradient distribution consists of a mixture of two harmonics. The first harmonic has a frequency equal to that of the wavy surface. The pressure gradient is negative in the regions where the inviscid flow accelerates, and it becomes positive in the regions where the flow decelerates. The maximum and minimum values of the pressure gradient

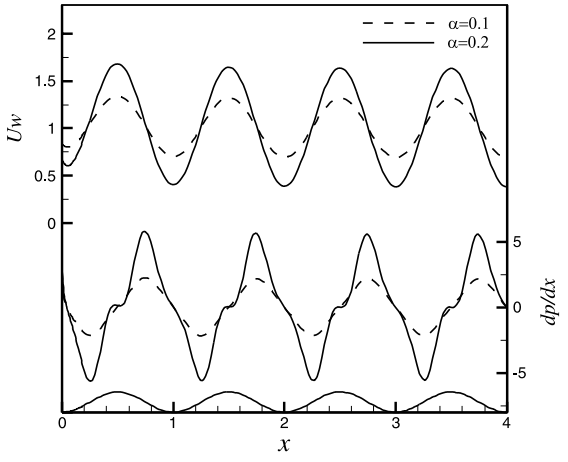

Fig. 2. Inviscid surface-velocity distribution and axial distribution of dp/dx.

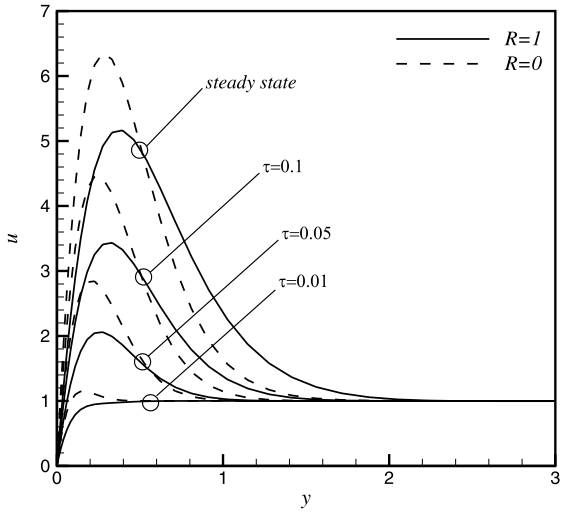

Fig. 3. Transient axial velocity profiles ($x = 2.75$).

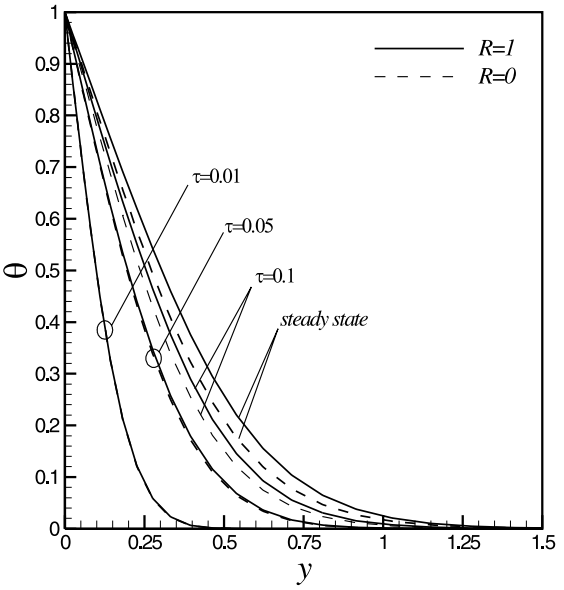

Fig. 4. Transient temperature distribution ($x = 2.75$).

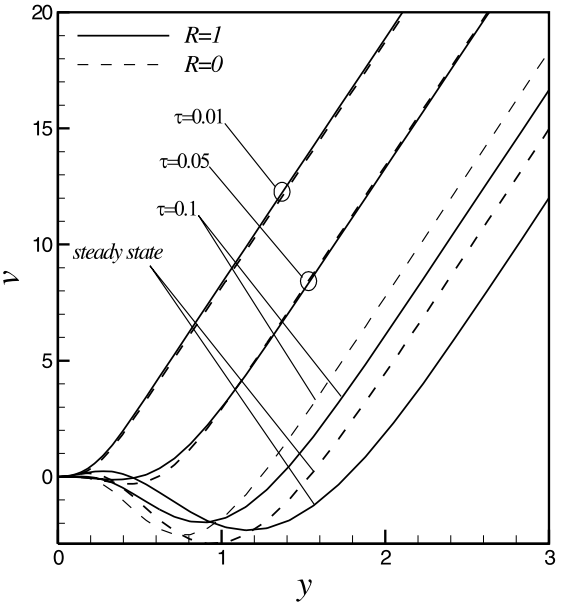

Fig. 5. Transient normal velocity profiles ($x = 2.75$).

occur at the points of inflection of the wavy surface. The pressure gradient increases with the amplitude–wavelength ratio. The present results for the x-component velocity of the inviscid flow and the pressure gradient are in good agreement with those obtained by Yao [16].

To verify the accuracy of the computer program used in this study, the steady-state results obtained for Newtonian fluid (i.e., $R = 0$) along wavy surface have been compared with those computed by Yao [16], as shown in Fig. 10. A favorable agreement is observed for the flow along a flat plate ($\alpha = 0$). However, for the flow along wavy surface, a smaller difference is found between the present results and those reported by Yao [16]. Note that the term $1 - xU_w/U'_w$ is presented in Eqs. (9a)–(9d) in this study, but this term does not exist in the report of Yao [16].

Figs. 3–6 display the results for the distribution of the transient axial velocity component u, temperature θ, normal velocity component v and microrotation N for the case of $Gr/Re^2 = 20\pi$, $\alpha = 0.1$, $\lambda = 5$, $x = 2.75$ (node), respectively. The axial velocity component and temperature increase with time at a given transverse position. These also show that the hydrodynamic and thermal boundary layers increase with time, and micropolar fluids have a thicker boundary layer than Newtonian fluid under any time.

Fig. 3 shows that because of the influence of buoyancy the axial velocity components of Newtonian and micropolar fluids grow with time. In a mixed-convection boundary layer, forced convection is the dominant mode of heat transfer at start time. And the axial velocity increases monotonically with time because of the cumulative free convection effect. However, the axial velocity component of micropolar fluid is smaller than that of the Newtonian fluid for transient and steady state. Because increasing the micropolar parameter results in an enhancement of the total viscosity in fluid flow, decreasing the axial velocity component.

Fig. 4 illustrates that the micropolar fluids have larger transient temperature. The transient axial velocity component of micropolar fluids is smaller than that of a Newtonian fluid as showed in Fig. 3; the smaller the axial velocity, the smaller the heat transfer rate. Because

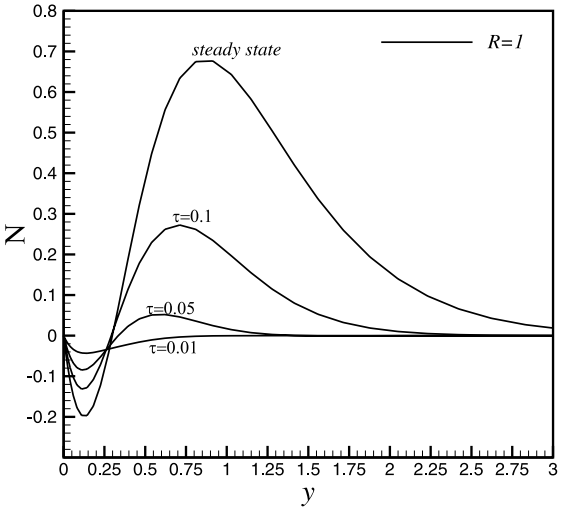

Fig. 6. Transient microrotation profiles ($x = 2.75$).

the temperature of the wavy surface is kept constant, the temperature profile becomes higher for micropolar fluids. This phenomenon reflects the fact that increasing the micropolar parameter results in an enhancement of the total viscosity in fluid flow, thus reducing the velocity and heat transfer rate.

The transformation from forced to free convection field can be seen more clearly in Fig. 5. As time is less than 0.05, the influence of buoyancy term is smaller, thus, the transient normal velocity component decreases gradually with time and increases with x. When time is larger than 0.1, buoyancy is the dominant mode, the negative normal velocity component can be found near $y = 1$. It should be noticed that negative normal velocity implies the direction is toward the surface, which is not normal to the wavy surface but is normal to the x-axis.

The transverse distribution of transient microrotation is plotted in Fig. 6. The amplitude of transient microrotation increases monotonically with time at the same transverse location except $y = 0.26$. The microrotation gradient $\partial N/\partial y$ near the wavy surface (i.e., $y < 0.1$) or far away from of the wavy surface is negative, which increases with time, and it becomes positive in the other region. Thus, the negative gradient $\partial N/\partial y$ in Eq. (9b) indicates the resistance force to decelerate flow as near wavy surface.

Figs. 7 and 8 plot the axial velocity component u, temperature θ as functions of the axial and transverse coordinates for $Gr/Re^2 = 20\pi, \lambda = 5, R = 5$ and $\alpha = 0.1$ at $\tau = 0.3$. The sinusoidal natures of the velocity and temperature field along the wavy surface are observed, which are more evident at a relatively small height from the surface. The amplitudes of the axial velocity component tend to increase as the fluid moves down-

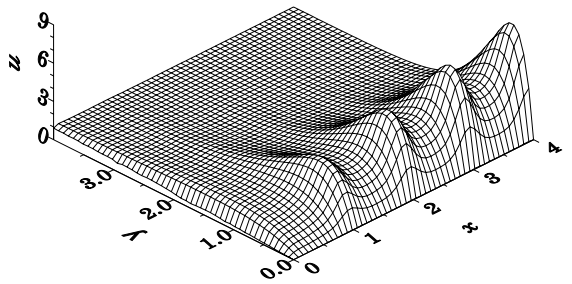

Fig. 7. Axial velocity profiles ($\alpha = 0.1, Gr/Re^2 = 20\pi, R = 5, \lambda = 5, \tau = 0.3$).

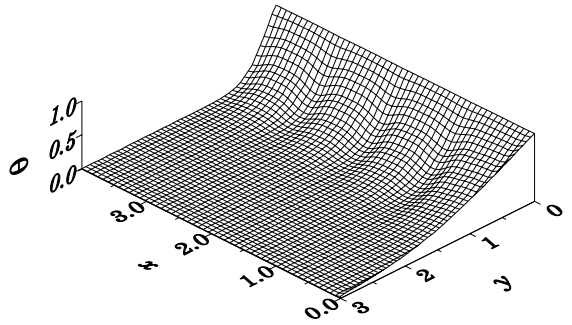

Fig. 8. Temperature profiles ($\alpha = 0.1, Gr/Re^2 = 20\pi, R = 5, \lambda = 5, \tau = 0.3$).

stream. The peaks of axial velocity component occur near the troughs of wavy surface (i.e., $x = 1, 2, 3$ and 4) where there are also the troughs of temperature field. In addition, forced convection is the dominant mode of heat transfer near the leading edge. And the axial velocity increases monotonically with x, but temperature decreases, because of the cumulative free convection effect.

Fig. 9 shows the variation of the transient local Nusselt number $(4/Gr_{\bar{x}})^{1/4}Nu_{\bar{x}}$ for the case of $\alpha = 0.1$, $Gr/Re^2 = 20\pi, \lambda = 5$, respectively. The transient local Nusselt number varies periodically. Its mean value decreases monotonically with the axial coordinate except near the leading edge; however, this mean value decreases with time. Forced convection controls the heat transfer mechanism initially, especially near the leading edge. As the time increases, the free convection effect becomes more pronounced, increasing the hydrodynamic and thermal boundary layer thicknesses, and thus reducing the heat transfer rate. Fig. 9 also shows that, for $\tau \leqslant 0.05$, the transient, local Nusselt number $(4/Gr_{\bar{x}})^{1/4}Nu_{\bar{x}}$ varies periodically with a frequency equal to the frequency of the wavy surface. The peaks of the transient, local heat transfer rate are found to be near the corresponding peaks of the wavy surface, where the maximum inviscid free-stream velocity is presented.

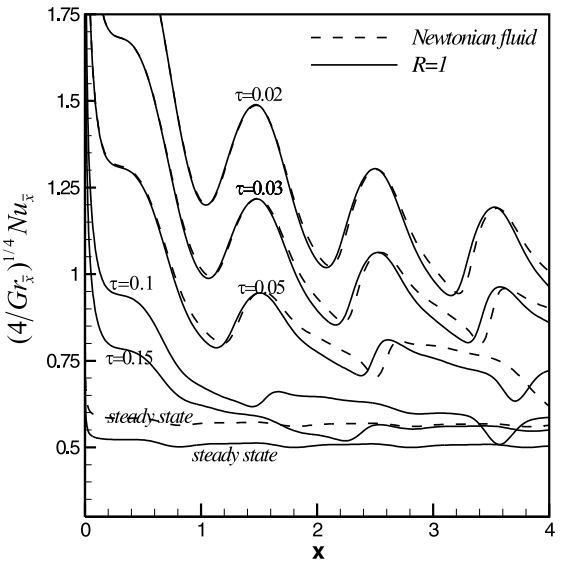

Fig. 9. Transient axial distribution of $(4/Gr_{\bar{x}})^{1/4}Nu_{\bar{x}}$ ($\alpha = 0.1$, $Gr/Re^2 = 20\pi, \lambda = 5$).

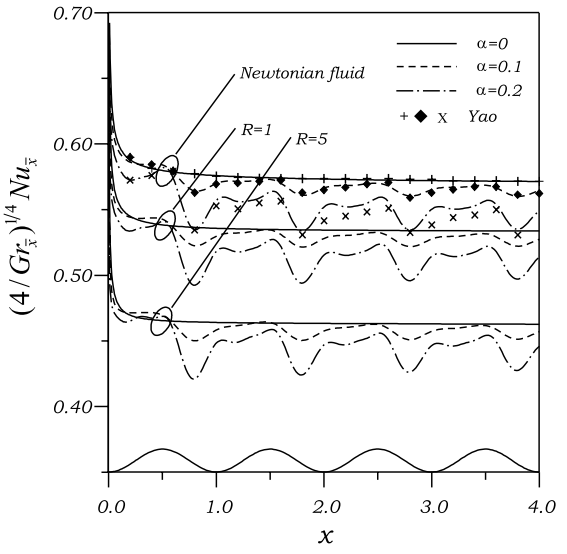

Fig. 10. Steady-state axial distribution of $(4/Gr_{\bar{x}})^{1/4}Nu_{\bar{x}}$ ($Gr/Re^2 = 20\pi, \lambda = 5$).

However, they shift slightly upstream of the crests of the wavy surface because of the non-linear convection effect.

The axial distribution of the steady state with local Nusselt number $(4/Gr_{\bar{x}})^{1/4}Nu_{\bar{x}}$ for different wavy amplitude–wavelength ratio and micropolar parameter is plotted in Fig. 10. The periodic nature of the local heat transfer rate is seen clearly in this figure. Yao concluded [7] that, in the steady state, local Nusselt number is a constant for the free convection flow along a flat plate in Newtonian fluids. In a mixed convection boundary layer, forced convection dominates the heat transfer near the leading edge, while free convection dominates the heat transfer as the fluid moves downstream. Hence, the steady state, local Nusselt number for the flat plate ($\alpha = 0$) decreases and then gradually levels off as the axis coordinate is increased.

The curves for $\alpha = 0.1$ and 0.2 in Fig. 10 indicate that the local Nusselt number distribution consists of two harmonics. The first harmonic is the leading-order forced convection solution, and the second harmonic is due to natural convection. As the axial coordinate increases, the mean value of $Nu_{\bar{x}}(4/Gr_{\bar{x}})^{1/4}$ is almost kept constant, except near the leading edge. As shown in Fig. 10, a micropolar fluid with large micropolar parameter has a low Nusselt number. This phenomenon reflects the fact that increasing the micropolar parameter results in an enhancement of the total viscosity in fluid flow, and thus the heat transfer is retarded.

The axial distribution of $(4/Gr_{\bar{x}})^{1/4}Nu_{\mathrm{m}}$ with x and R is plotted in Fig. 11 for $Gr/Re^2 = 20\pi, \alpha = 0.1$, $B = 1$, $\lambda = 5$ and $Pr = 1$. The total Nusselt number is obtained

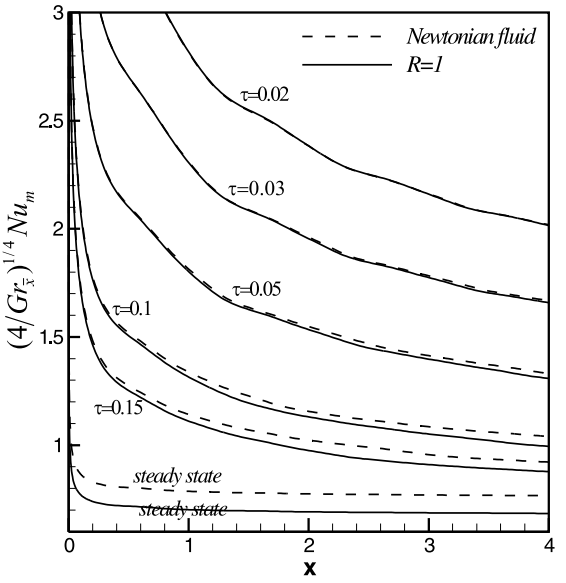

Fig. 11. Transient axial distribution of $(4/Gr_{\bar{x}})^{1/4}Nu_{\mathrm{m}}$ ($\alpha = 0.1$, $Gr/Re^2 = 20\pi, \lambda = 5$).

by averaging the heat transfer rate over the surface from the leading edge to $\sigma(x)$ which is expressed in Eq. (12b). It shows that the total Nusselt number of the wavy surface decreases with time and x. Further, in transient and steady states, the Newtonian fluid is found to have higher averaged heat transfer rate than a micropolar fluid.

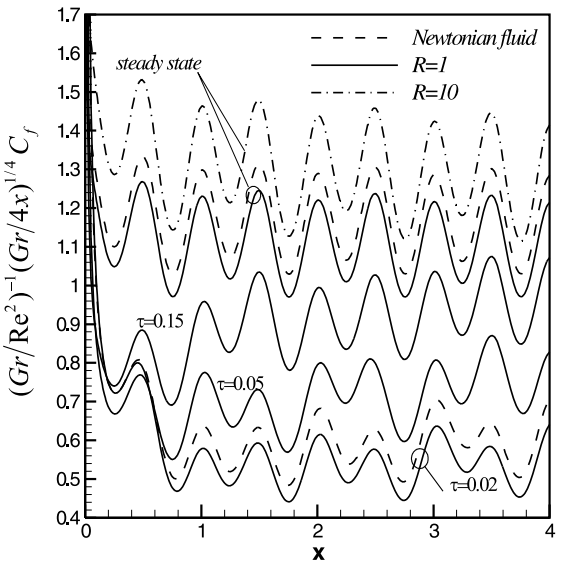

Fig. 12. Transient axial distribution of $(Gr/Re^2)^{-1}(Gr/4x)^{1/4}C_f$ $\alpha = 0.1, Gr/Re^2 = 20\pi, \lambda = 5$).

Fig. 12 shows the growth of the transient skin friction coefficient for $Gr/Re^2 = 20\pi$, $\lambda = 5$ and $\alpha = 0.1$. It shows that, in a mixed-convection boundary layer, forced convection dominates over natural convection at smaller time. Therefore, the skin friction coefficient increases with time until arriving steady state and shows the presence of two harmonics under larger time. The peaks of the first harmonic occur near the peaks of the wavy surface, and the quantity of amplitude is almost constant as $\tau > 0.02$ (i.e., the amplitude does not grow). The peaks of the second harmonic occur near the troughs of wavy surface and grow with time until arriving steady state. This is because the buoyancy term in Eq. (9b) increases with time and accelerates the fluid along the surface, thus the second harmonic becomes prominent at large time. On the other hand, the skin friction coefficient for vortex viscosity parameter $R = 1$ in micropolar fluid is smaller than the Newtonian fluid, but as increasing vortex viscosity parameter to $R = 10$ the skin friction coefficient becomes bigger than the Newtonian fluid.

5. Conclusion

The theory of micropolar fluids has been used to derive a numerical transient solution for flowing along a wavy surface in a mixed convection. Prandtl's transposition theorem and the spline alternating-direction implicit method have been applied to solve the problem.

The hydrodynamic and thermal boundary layer thicknesses increase progressively with the time. As the time increases, the local skin-friction coefficient increases but the local and averaged heat transfer rates decrease which shows the presence of two harmonics. Forced convection dominates the first harmonic at smaller time or near the leading edge, while free convection dominates the second harmonic as the time increases or fluids move downstream. In micropolar fluids, the skin friction coefficient is lower than Newtonian fluids for smaller vortex viscosity parameter, but higher for larger vortex viscosity parameter. However, the heat transfer rate decreases because of smaller axial velocity for micropolar fluids. Thus, the heat transfer rate of a micropolar fluid is smaller than a Newtonian fluid under all circumstances.

References

[1] A.C. Eringen, Theory of micropolar fluids, J. Math. Mech. 16 (1) (1966) 1–16.
[2] T. Ariman, M.A. Turk, N.D. Sylvester, Microcontinuum fluid mechanics – a review, Int. J. Eng. Sci. 11 (8) (1973) 905–930.
[3] T. Ariman, M.A. Turk, N.D. Sylvester, Applications of microcontinuum fluid mechanics, Int. J. Eng. Sci. 12 (4) (1974) 273–293.
[4] G. Ahmadi, Self-similar solution of incompressible micropolar boundary layer flow over a semi-infinite plate, Int. J. Eng. Sci. 14 (7) (1976) 639–646.
[5] T.Y. Wang, C. Kleinstreuer, Thermal convection on micropolar fluids past two-dimensional or axisymmetric bodies with suction/injection, Int. J. Eng. Sci. 26 (1988) 1267–1277.
[6] H.S. Takhar, R.S. Agarwal, R. Bhargava, S. Jain, Mixed convection flow of a micropolar fluid over a stretching sheet, Heat Mass Transfer/Waerme- und Stoffuebertragung 34 (2) (1998) 213–219.
[7] L.S. Yao, Natural convection along a vertical wavy surface, ASME J. Heat Transfer 105 (3) (1983) 465–468.
[8] L.S. Yao, A note on Prandtl's transposition theorem, ASME J. Heat Transfer 110 (2) (1988) 503–507.
[9] S.G. Moulic, L.S. Yao, Natural convection along a vertical wavy surface with uniform heat flux, ASME J. Heat Transfer 111 (1989) 1106–1108.
[10] D.A.S. Rees, I. Pop, A note on free convection along a vertical wavy surface in a porous medium, ASME J. Heat Transfer 116 (2) (1994) 505–508.
[11] I. Pop, T.Y. Na, Natural convection of a Darcian fluid about a wavy cone, Int. Commun. Heat Mass Transfer 21 (6) (1994) 891–899.
[12] S.D. Harris, D.B. Ingham, I. Pop, Transient free convection from a vertical plate subjected to a change in surface heat flux in porous media, Fluid Dyn. Res. 18 (1996) 313–324.
[13] J.J. Shu, I. Pop, Transient conjugate free convection from a vertical flat plate in a porous medium subjected to a sudden change in surface heat flux, Int. J. Eng. Sci. 36 (2) (1998) 207–214.

[14] C.P. Chiu, H.M. Chou, Free convection in the boundary layer flow of a micropolar fluid along a vertical wavy surface, Acta Mech. 101 (1993) 161–174.
[15] C.P. Chiu, H.M. Chou, Transient analysis of natural convection in along a vertical wavy surface in micropolar fluid, Int. J. Eng. Sci. 32 (1) (1994) 19–33.
[16] S.G. Moulic, L.S. Yao, Mixed convection along a vertical wavy surface, ASME J. Heat Transfer 111 (1989) 974–978.
[17] S.G. Rubin, R.A. Graves, Viscous flow solution with a cubic spline approximation, Comput. Fluids 1 (1975) 1–36.
[18] P. Wang, R. Kahawita, Numerical integration of partial differential equations using cubic spline, Int. J. Comput. Math. 13 (3) (1983) 271–286.
[19] M.I. Char, C.K. Chen, Temperature field in non-Newtonian flow over a stretching plate with variable heat flux, Int. J. Heat Mass Transfer 31 (5) (1988) 917–921.